Naval Surface Warfare Center
Carderock Division
9500 MacArthur Boulevard, West Bethesda, MD 20817-5700

NSWCCD-50-TR–2000/016 March 2000

Hydromechanics Directorate Report

RANS ANALYSIS OF FREE-SURFACE AND BOTTOM EFFECTS ON AXISYMMETRIC RCMS

by

Henry J. Haussling and Roderick M. Coleman

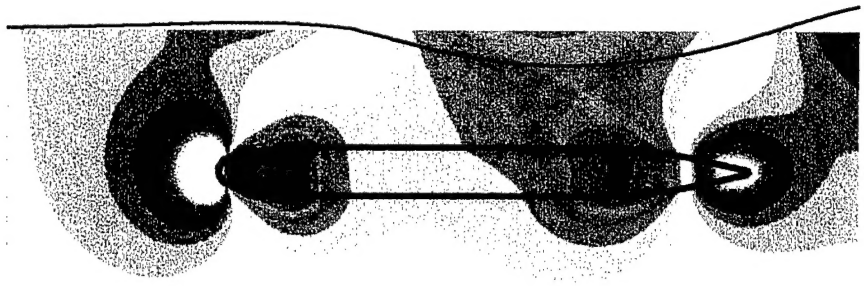

NSWCCD-50-TR–2000/016 RANS Analysis of Free-Surface and Bottom Effects on Axisymmetric RCMs

REPORT DOCUMENTATION PAGE

Form Approved OMB No. 0704-0188

1. AGENCY USE ONLY *(Leave blank)*	2. REPORT DATE	3. REPORT TYPE AND DATES COVERED
	March 2000	Final 1/99-12/99

4. TITLE AND SUBTITLE
RANS Analysis of Free-Surface and Bottom Effects on Axisymmetric RCMs

5. FUNDING NUMBERS
WU: 5600-259

6. AUTHOR(S)
Henry J. Haussling and Roderick M. Coleman

7. PERFORMING ORGANIZATION NAME(S) AND ADDRESS(ES)
Naval Surface Warfare Center
Carderock Division
9500 MacArthur Boulevard
West Bethesda, MD 20817-5700

8. PERFORMING ORGANIZATION REPORT NUMBER
NSWCCD-50-TR-2000/016

9. SPONSORING/MONITORING AGENCY NAME(S) AND ADDRESS(ES)

10. SPONSORING/MONITORING AGENCY REPORT NUMBER

11. SUPPLEMENTARY NOTES

12a. DISTRIBUTION CODE

12b. DISTRIBUTION/AVAILABILITY STATEMENT
Approved for Public Release, Distribution Unlimited.

13. ABSTRACT ***(Maximum 200 words)***

The UNCLE Reynolds-averaged Navier-Stokes code is used to investigate free-surface and bottom effects on an axisymmetric radio-controlled submarine model. It is shown that the basin bottom and water surface have small but noticeable influences on the hydrodynamic vertical force and pitching moment on the body for typical depths of submergence. The influence of submergence depth and speed on the forces and moments is analyzed. It is shown that the presence of the water surface leads to vertical velocities near the stern that are consistent with sternplane deflections previously found necessary to keep appended models in straight and level motion.

14. SUBJECT TERMS
Navier-Stokes equations
submarine hydrodynamics
free surface
radio-controlled model

15. NUMBER OF PAGES
26

16. PRICE CODE

17. SECURITY CLASSIFICATION OF REPORT	18. SECURITY CLASSIFICATION OF THIS PAGE	19. SECURITY CLASSIFICATION OF ABSTRACT	20. LIMITATION OF ABSTRACT
UNCLASSIFIED	UNCLASSIFIED	UNCLASSIFIED	UL

NSN 7540-01-280-5500

Standard Form 298 (Rev. 2-89)
Prescribed by ANSI Std. Z39-18
298-102

CONTENTS

FIGURES

TABLES

ABSTRACT

The UNCLE Reynolds-averaged Navier-Stokes (RANS) code is used to investigate free-surface and bottom effects on an axisymmetric radio-controlled submarine model. It is shown that the basin bottom and water surface have small but noticeable influences on the hydrodynamic vertical force and pitching moment on the body for typical depths of submergence. The influence of submergence depth and speed on the forces and moments is analyzed. It is shown that the presence of the water surface leads to vertical velocities near the stern that are consistent with sternplane deflections previously found necessary to keep appended models in straight and level motion.

ADMINISTRATIVE INFORMATION

This investigation was sponsored by the Naval Sea Systems Command, Code PM0450, Task Area F1947 through Work Request WR10453 dated 25 Oct 99, under work unit number 1-5600-259. The work was performed by the Hydromechanics Directorate, Code 54, Carderock Division Headquarters, Naval Surface Warfare Center (NSWCCD).

INTRODUCTION

Radio-controlled tests of submarine models (RCM tests) are carried out at Naval Surface Warfare Center, Carderock Division (NSWCCD) in a test basin with a water depth of 20 feet (6.096 meters). It has been noted that sternplane deflections are necessary to maintain straight and level motion. The amount of deflection necessary depends on the depth of the model. This indicates that the presence of the basin bottom and/or the free water surface is having an effect on the model performance. A similar effect has been noted in near-surface tests of the Large Scale Vehicle (LSV).[1]

A simplified source potential flow model was used to analyze this free surface effect.[2] From that study, it was concluded that the effect is predominantly due to a normal wash on the sternplanes which results from the hull/free-surface interaction. Recent advances in Reynolds-averaged Navier-Stokes (RANS) equations computational solution techniques now allow a similar analysis with fewer approximations.

The current study assesses free-surface and bottom effects on the vertical force and the pitching moment of an axisymmetric body as well as on the local angle of attack in the stern area. The scalably-parallel UNCLE Reynolds-averaged Navier-Stokes (RANS) code, Release 1.2, is used. This software has been, and continues to be, developed at Miss. State Univ. with support from the Office of Naval Research. An earlier version of UNCLE was used to assess bottom effects on model performance.[3] For models with distances from the basin bottom to the keel ranging from 7 model diameters to 0.7 diameters, it was found that the hydrodynamic coefficients varied less than 10%. The

addition of free-surface boundary conditions in this recent code release allows free-surface effects to be assessed as well. This advance also makes feasible the prediction of submarine maneuvering performance when neither viscous nor water surface effects can be neglected.

BOUNDARY CONDITIONS, GRID AND FORCES

The UNCLE code requires that the vertical coordinate be Y when free surface conditions are applied. However, in recording the results of this study in this report Z is used as the vertical coordinate to conform to submarine maneuvering conventions.

A block-shaped computational region is defined. An upstream boundary is one body length upstream of the nose ($X/L = -1.0$). A downstream boundary is two body lengths downstream from the stern ($X/L = 3.0$). A side boundary is one body length from the centerplane ($Y/L = 1.0$). UNCLE's characteristic far-field boundary conditions are applied on these three boundaries. At the centerplane, above and below the body, ($Y/L = 0.0$) symmetry conditions are applied. No-slip wall conditions are applied at the basin bottom ($Z/L = -0.8812$). However, accurate resolution of the boundary layer on this wall is not attempted.

Three submergence depths are considered corresponding to distances from the water surface to the keel of 7, 10 and 13 feet (2.1336, 3.048, and 3.9624 meters). These correspond to distances from the water surface to the body centerline of about 2.9, 4.4 and 5.9 body diameters, respectively. Nonslip wall conditions are applied on the hull surface with boundary layer resolution.

The undisturbed water surface is at $Z/L = 0.0$. Inviscid free-surface conditions are applied. The pressure (dynamic plus hydrostatic) is atmospheric (defined to be zero) at the actual water level $Z = H$. The height H is computed from the kinematic condition that there be no flow across the free surface. These free-surface conditions are linearized by applying them at $Z = 0.0$ rather that at $Z = H$. This linearization allows all computations to be carried out on a fixed grid. Fully nonlinear computations with grid adjustment can be carried out by UNCLE but are unnecessary for these flows where wave slopes are quite small and the linearization is an excellent approximation.

A cross section of the grid is displayed in Figure 1. Block boundaries are shown by thick lines. A cylindrical grid near the body is imbedded in a rectangular grid to fit the outer boundaries. There are about 2.85 million grid points in all, divided into 70 blocks for parallel processing. This is a rather large grid for half of an axisymmetric body but extra points are needed to conform to the bottom and free-surface boundaries, to resolve the high-frequency waves that are present on the water surface when the speed is low, and to obtain accurate integrated force values.

The grid on the centerplane is displayed in Figure 2. There are 193 points along the body in the streamwise direction and 65 wrapping around it. Typical boundary layer spacing is present on the body surface aiming at $y^+ = 1$ for the first grid surface off the body. Some vertical clustering is also present at the water surface and basin bottom.

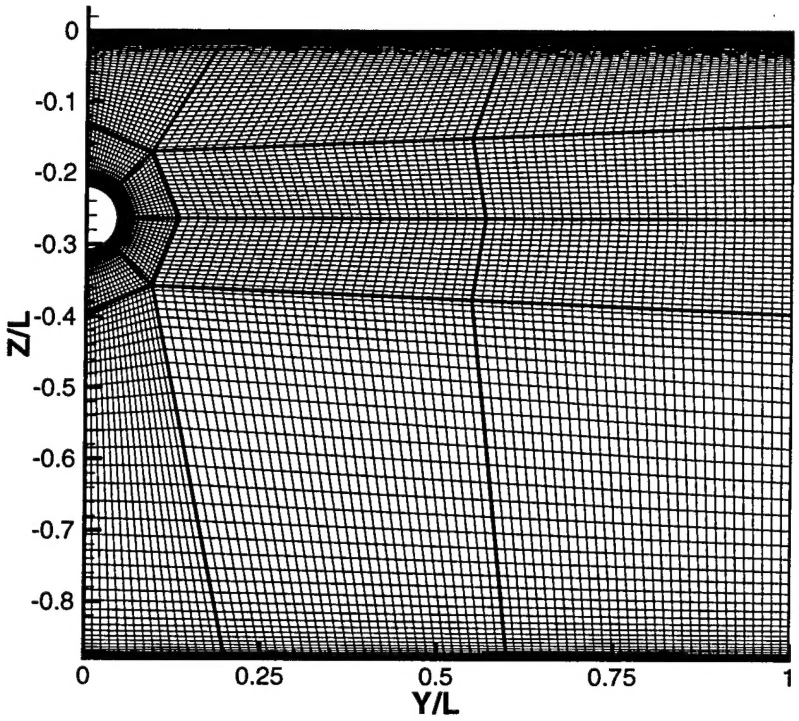

Fig. 1. A typical grid cross section.

The version of the UNCLE code used integrates the nondimensional pressure and viscous stresses per unit area to obtain nondimensional forces. These quantities are multiplied by a factor of two to obtain the usual force coefficients (X', Y', Z') normalized by $\rho U^2 L^2/2$ and moment coefficients (K', M', N') normalized by $\rho U^2 L^3/2$. A second factor of two is applied to account for the forces and moments on the half of the hull that is not present in the symmetric computation.

RESULTS

Body in an infinite fluid

The force and moment coefficients of interest are rather small with typical values on the order of 10^{-5}. Thus it is necessary that the computed flow solution and the force integration be quite accurate. In order to gain confidence that the code and the grid can be used to predict such small forces, the case of a body in a basin of infinite vertical extent is first computed. The grid for the depth of 10 feet (3.048 meters) is employed and farfield boundary conditions are applied at the top and bottom boundaries. The vertical force and pitching moment on such an axisymmetric body will be zero. The

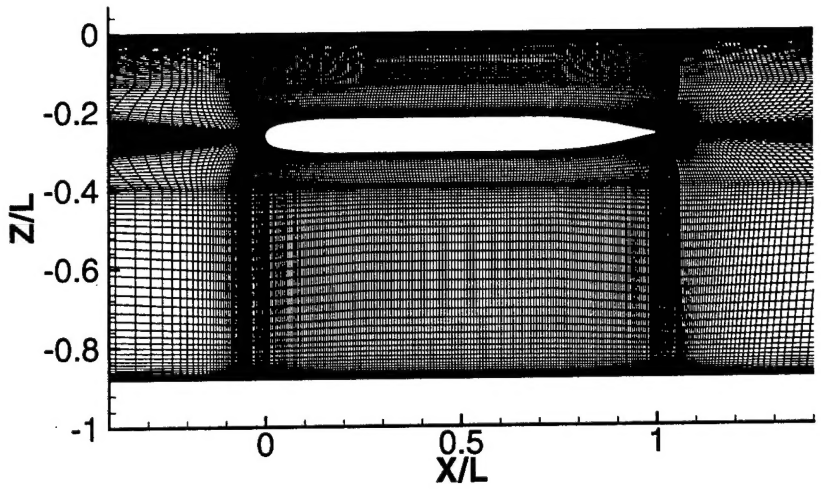

Fig. 2. Grid in the centerplane.

predicted force and moment will represent combined error due to the code, the grid, and the farfield conditions. If the error is comparable to the forces and moments of interest we have a problem. In such a case, unless the error can be reduced by moving the outer boundaries farther away, the use of the code for the current purpose is not possible.

This infinite depth case is run with Reynolds number (based on body length and speed) of $Re = 25.6 \times 10^6$ for 750 cycles using a CFL number (computational step size) of 10. The force and moment history are presented in Figure 3. It can be seen that the force and moment converge very quickly to very small values - on the order of 10^{-7}. Thus there is hope that the current grid can be used to compute forces and moments on the order of 10^{-5}.

For comparison with later results, the predicted pressure coefficient on the body and on the centerplane for the infinite depth case is presented in Figure 4. To the naked eye, the Cp distribution appears symmetric vertically, even though the grid is not symmetric because the body is somewhat closer to the top farfield boundary than to the bottom farfield boundary.

Depth 7

Computations are carried out for depth 7 with free-surface boundary conditions on the upper boundary and a wall condition on the lower boundary with $Re = 25.6 \times 10^6$. This corresponds to a Froude number (Fr, based on body length and speed) of 0.459. This case was started at cycle 3000 from a previous test run at a lower speed. The force and moment convergence histories are displayed in Figure 5. They indicate convergence to values of about $Z' = -12.97 \times 10^{-5}$ and $M' = -6.09 \times 10^{-5}$. There is an upward force and a bow down pitching moment.

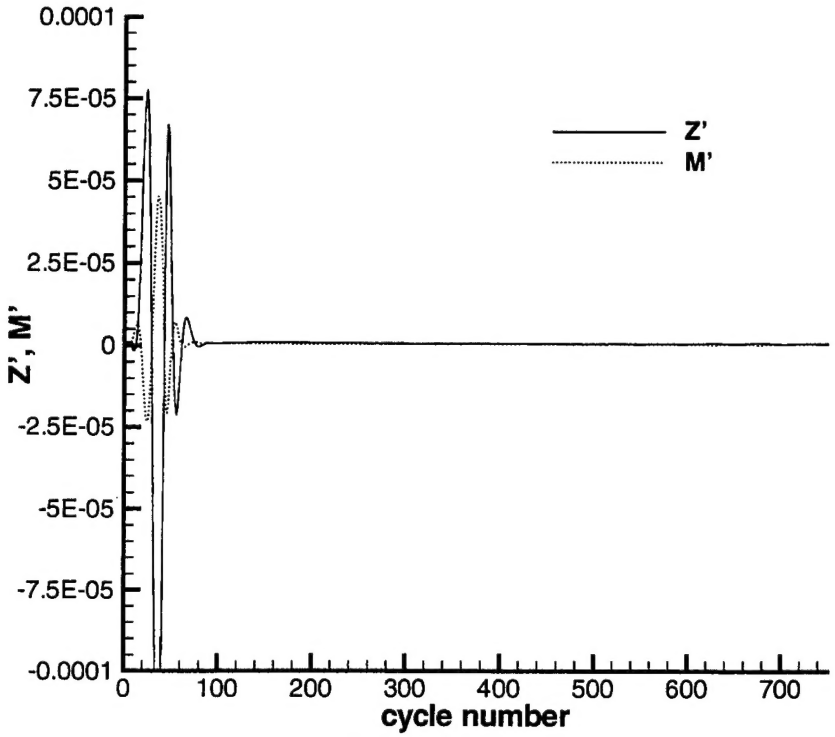

Fig. 3. Computed force and moment vs. cycle number for body in a basin of infinite vertical extent.

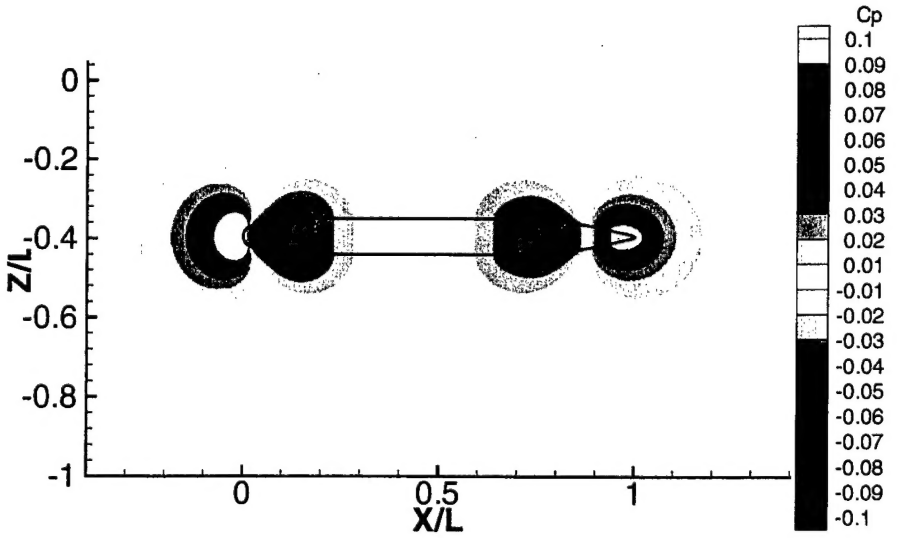

Fig. 4. Predicted pressure coefficient on the body and centerplane for a basin of infinite vertical extent.

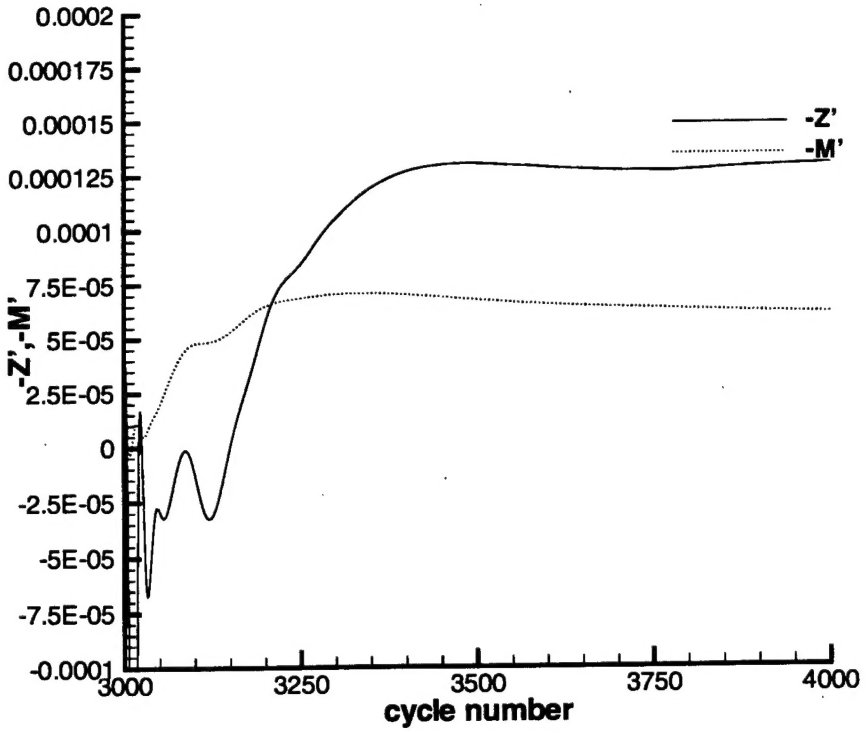

Fig. 5. Computed force and moment vs. cycle number for depth 7 and $Fr = 0.459$.

The predicted waves are shown in Figure 6. There is a bow wave of height about 0.002 boat lengths (about 0.022 diameters), a midship trough of depth about 0.006 boat lengths centered at $X/L = 0.65$, a lagging stern wave of height about 0.006 centered at $X/L = 1.35$ and a trailing wave train. The theoretical wavelength of about 1.3 boat lengths for this Froude number is well represented.

The pressure coefficient on the hull and centerplane is displayed in Figure 7. It can be seen that the waves lead to an increased pressure near the bow, associated with the bow wave, an increased pressure at the stern, associated with the stern wave, and a decreased pressure over about 50% of the body beginning at about $X/L = 0.3$.

Plots of the pressure coefficient on the top and bottom of the body are presented in Figure 8. Pressure differences result from the fact that the free-surface effects are greater on the top than on the bottom of the body. These differences lead to downward force on roughly the first 30% of the body, an upward force an the next 50% and then some downward force on the remaining 20%. The effect of this force distribution is the net upward force and the bow down pitching moment mentioned above. A key to the magnitude of the force and moment is that the speed is high enough that the waves are shifted somewhat downstream, that the effect of the stern wave on the body is thus reduced, and that the effect of the midship trough is large and thus dominates so much of the body, particularly downstream of the center of gravity.

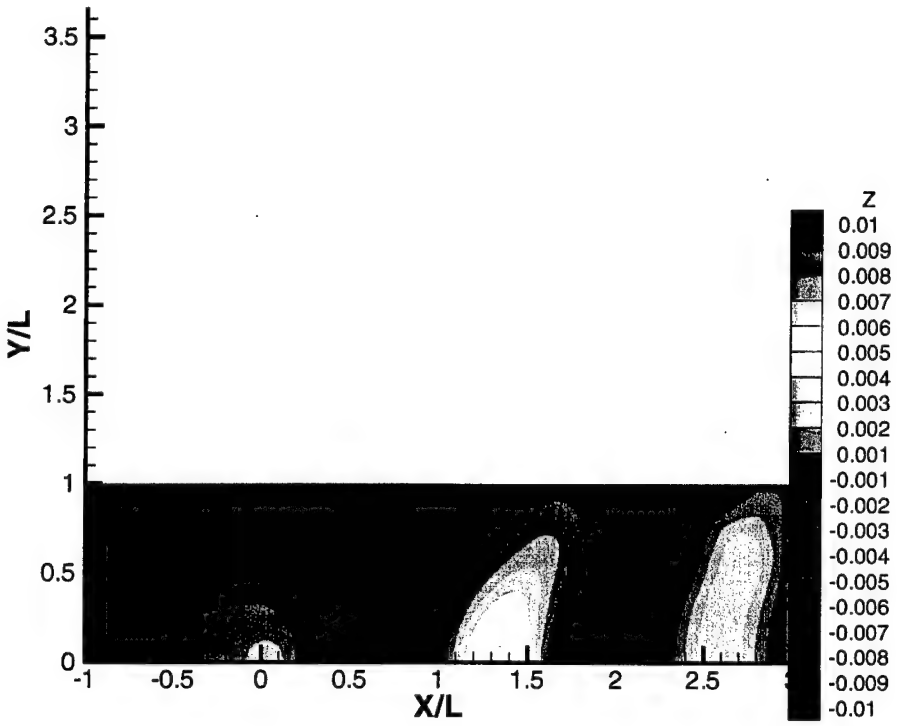

Fig. 6. Computed surface wave pattern for depth 7 and $Fr = 0.459$.

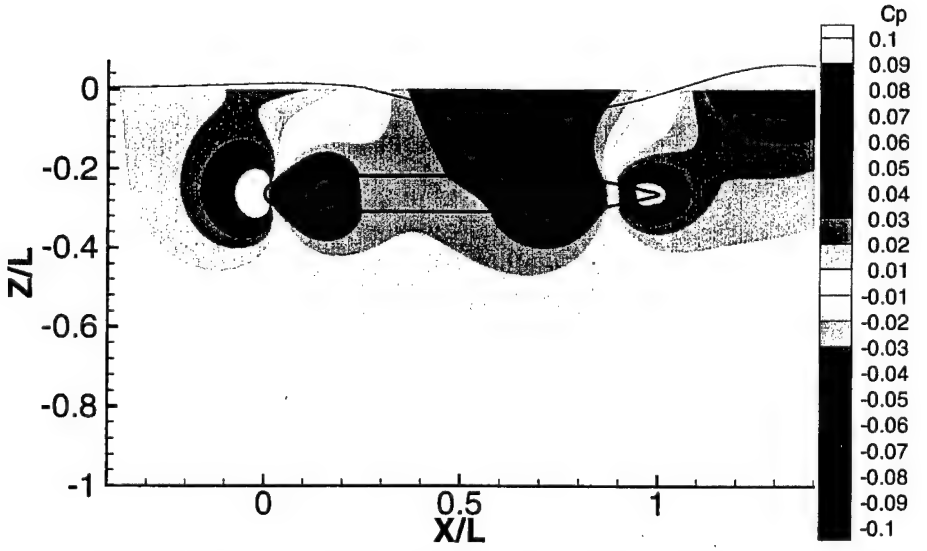

Fig. 7. Computed pressure coefficient on the hull and centerplane for depth 7 and $Fr = 0.459$. Also shown is the free surface deformation magnified 10 times.

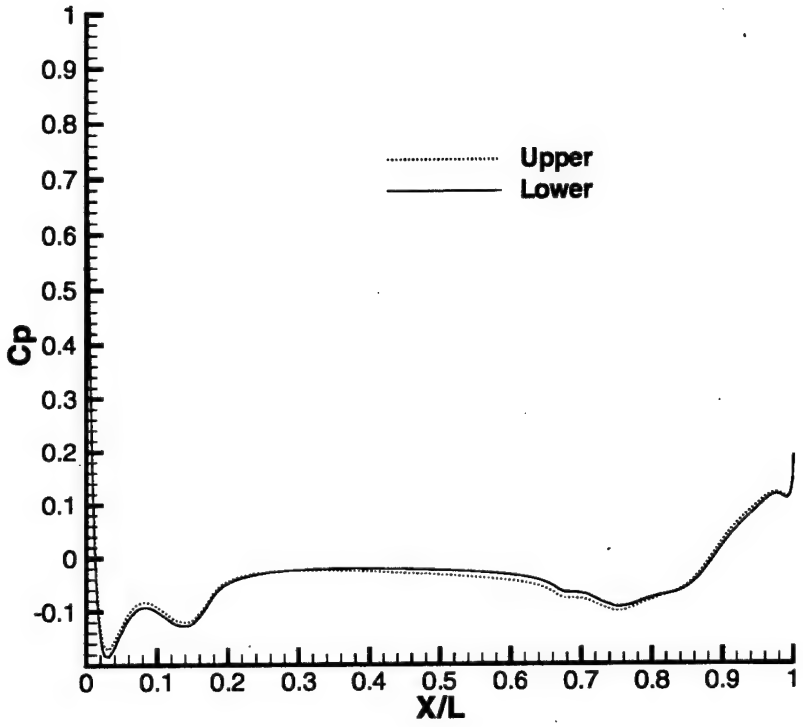

Fig. 8. Computed pressure coefficient on the upper and lower intersections of the body with the centerplane for depth 7 and $Fr = 0.459$.

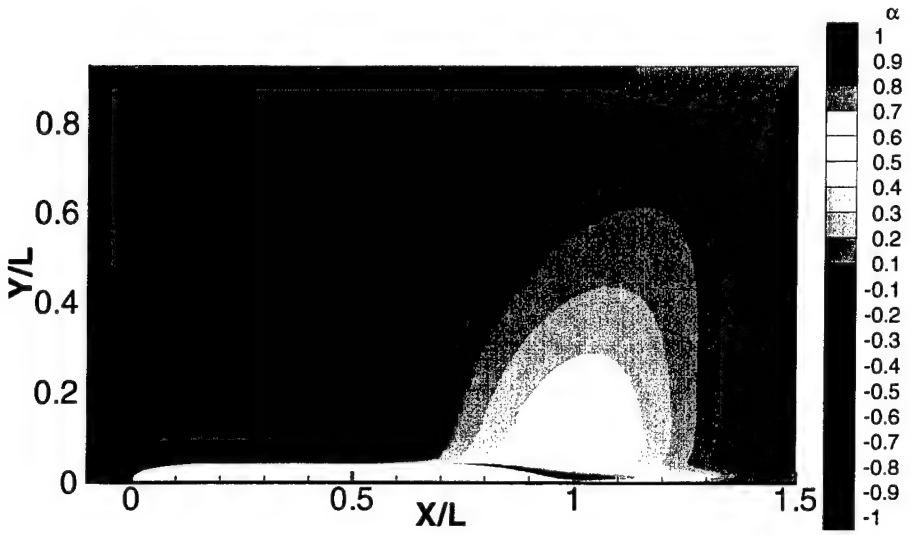

Fig. 9. Computed local angle of attack α^o in the horizontal centerplane for depth 7 and $Fr = 0.459$.

The local angle of attack, $tan^{-1}(w/u)$, in the horizontal centerplane is displayed in Figures 9 and 10. It is seen that there is a downwash near the bow and an upwash near the stern which are directly connected to the bow and stern waves. The angle of attack reaches values of around 1 degree near the stern. This is large enough to account for the sternplane deflections, on the order of 1 degree, which are necessary to keep the RCM straight and level when near the water surface.

The slower speeds of interest, for depth 7, are computed in five successive runs, each started from the solution for the next higher speed. Each case is run for 750 cycles. The force and moment histories are presented in Figure 11. It is seen that the forces and moments converge nicely for the two higher speeds. However, for lower speed the convergence becomes oscillatory. In fact, for $Fr = 0.077$ (not shown), large-amplitude, high-frequency waves develop on the water surface and the force and moment show no indication of convergence after 750 iterations. The reason for the difficulties in computing the slower speeds is the existence of the very high frequency (short wavelength) waves. The values of the force and moment computed are presented in Table 1. The values for depth 7 at $Fr = 0.077$ are obtained from the double model solution, a good appoximation as discussed below. As the speed decreases the force and moment for depth 7 both decrease in magnitude.

The computed centerline wave profiles for these four speeds are presented in Figure 12. The wave amplitude decreases and the frequency increases as the speed decreases. Also shown is a wave profile computed from a double model solution for depth 7. Such a solution is obtained by applying an inviscid wall condition at the water surface in place of the free surface conditions. It is known that the free surface solution approaches a rigid wall solution asymptotically as the speed approaches zero. In addition, the

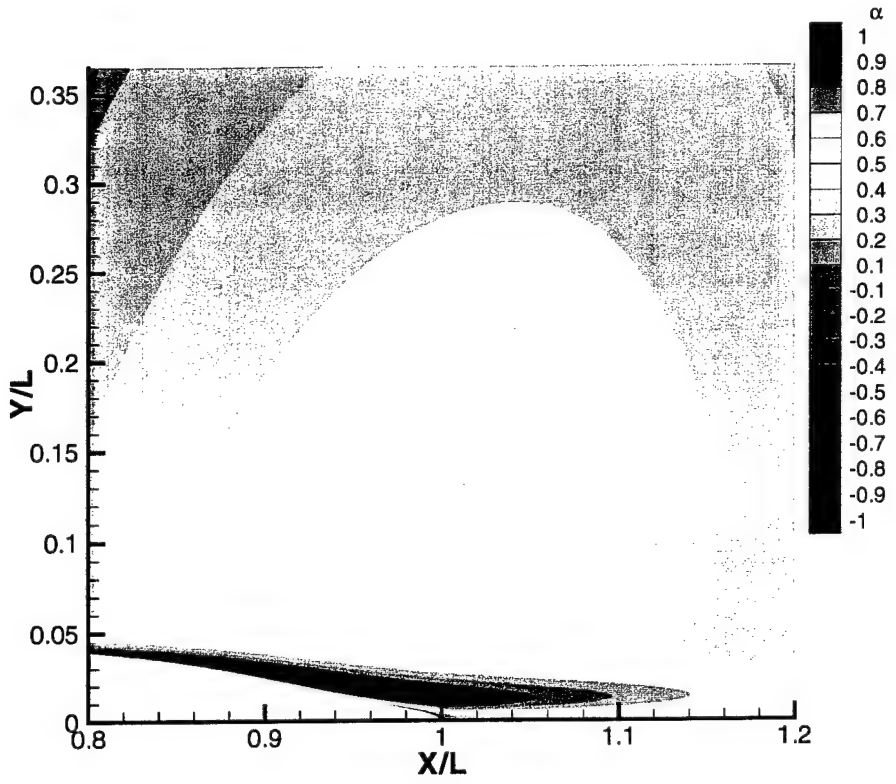

Fig. 10. Computed local angle of attack α^o near the stern in the horizontal center plane for depth 7 and $Fr = 0.459$.

	depth					
	7		10		13	
Fr	$Z'x10^5$	$M'x10^5$	$Z'x10^5$	$M'x10^5$	$Z'x10^5$	$M'x10^5$
0.077	-3.90	-0.0965	-0.636	0.0084	1.27	0.0855
0.153	-3.96	-0.0390	-0.636	0.0084	1.27	0.0855
0.230	-4.85	-0.0960	-1.07	-0.017	1.10	0.12
0.306	-6.40	-0.151	-1.49	-0.019	0.96	0.085
0.383	-9.96	-1.12	-2.49	-0.175	0.64	0.036
0.459	-13.79	-5.93	-4.24	-1.41	-0.080	-0.31

Table 1. Computed vertical forces and pitching moments.

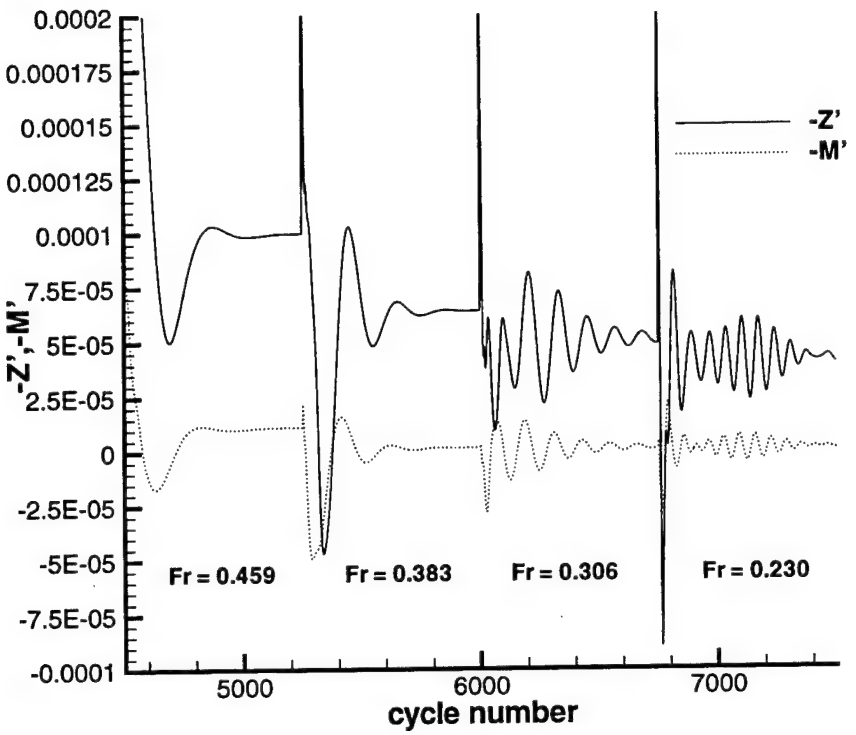

Fig. 11. Computed force and moment histories for depth 7 and four speeds.

free surface height approaches the surface pressure P multiplied by Fr^2. Indeed, it is noted in Figure 12 that the computed wave elevation for $Fr = 0.153$ is very well approximated by such an estimate from the double-model solution. This means that the free-surface effect is essentially the same as the effect of a wall for Fr less than about 0.15. Thus, the magnitude of the force and moment decrease as the waves diminish with decreasing speed, and approach asymptotically the force and moment due to the presence of a wall, which are relatively small and speed independent. Similarly the local angle of attack distribution in the horizontal centerplane is shifted and diminished with decreasing speed.

Depth 10

Computations are carried out for depth 10 at four speeds. The highest speed is run first. Each case is computed for 750 cycles and each is started from the solution for the next higher speed. $CFL = 10.0$ is used for the three highest speeds but $CFL = 5.0$ is used for $Fr = 0.230$ in an attempt to suppress the high-frequency oscillations noted at the lower speeds for depth 7. The force and moment histories are presented in Figure 13. The forces and moments converge quite well for the three highest speeds. For $Fr = 0.230$ oscillations are present once more. Although they are of smaller amplitude than for the same speed at depth 7, they are only slowly decaying. For

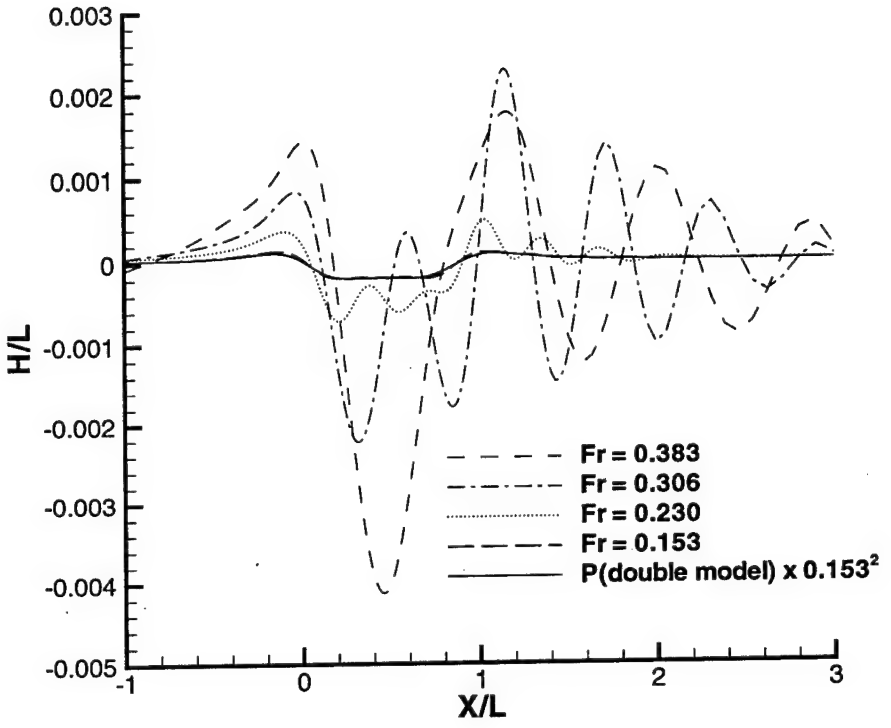

Fig. 12. Computed centerline wave profiles for depth 7 and four speeds compared with a profile obtained from a double model solution.

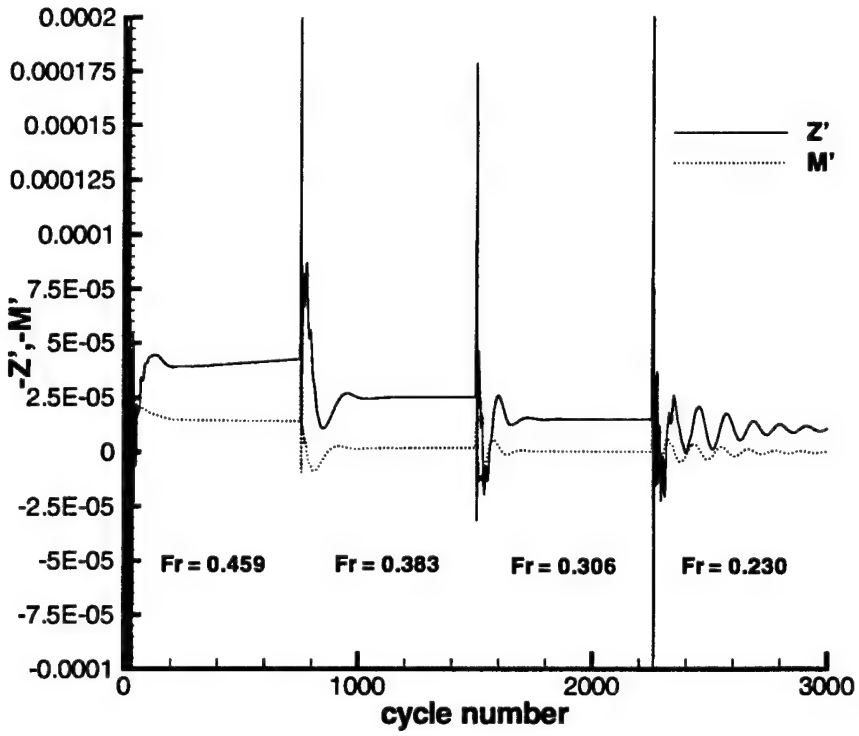

Fig. 13. Computed force and moment histories for depth 10 and four speeds.

$Fr = 0.153$ and $Fr = 0.077$ the computations showed no sign of converging during the 750 cycles attempted. Separate computational experiments showed that converged free surface solutions can be obtained at these very slow speeds but they must be run for many cycles to allow the high frequency disturbances to decay. Fortunately it is not necessary to compute such cases due to the accuracy of the double model approximation.

The predicted wave pattern for $Fr = 0.459$ is shown in Figure 14. The same color scale is used as in Figure 6 so that a direct comparison demonstrates that the wave amplitude in this case is much lower than for the shallower submergence. Because of the lower wave heights, the local angle of attack distribution is diminished in amplitude.

Centerplane wave profiles for the four speeds are compared in Figure 15. It is seen that for this submergence the double model solution is quite good already at $Fr = 0.23$.

Depth 13

Computations are carried out for depth 13 at four speeds. The highest speed is run first. Each case is computed for 750 cycles with $CFL = 10.0$ and each is started from the solution for the next higher speed. The force and moment histories are presented in Figure 16. The forces and moments converge quite well for all four speeds. At this deepest submergence, the free-surface effect on the forces is seen to be much reduced, but still present. It can also be noted that the force Z' is positive because of the

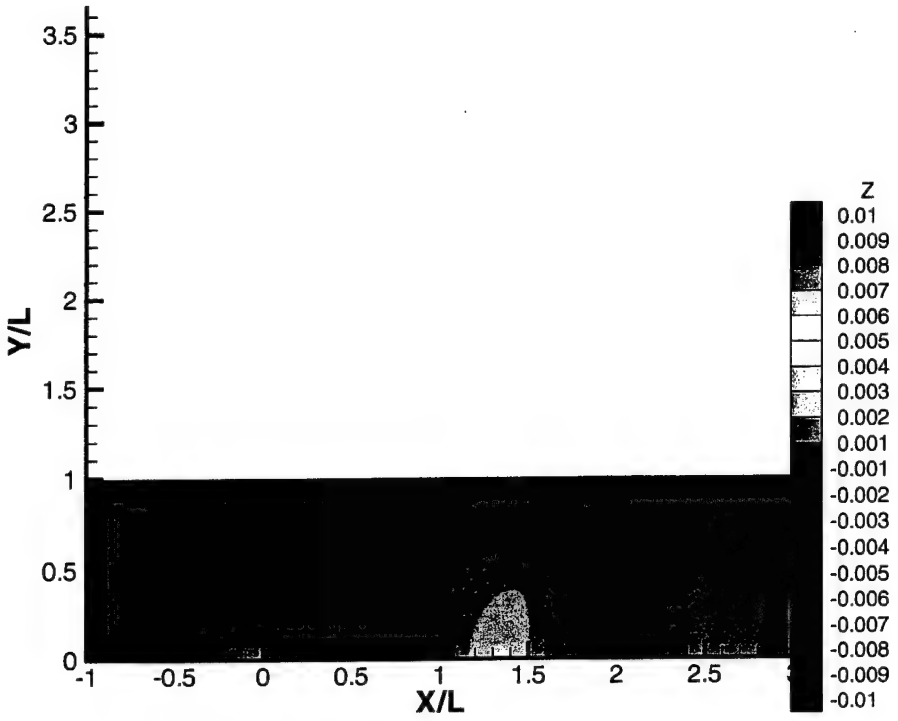

Fig. 14. Computed surface wave pattern for depth 10 and $Fr = 0.459$.

downward attraction to the tank bottom.

Centerplane wave profiles for the six speeds are compared in Figure 17. For this deep submergence the largest deviation of the water surface from its undisturbed level is only 0.2% of the body length. The surface elevation for $Fr = 0.230$ is once again almost identical to the double model solution. The waves in Figure 17 are remarkably similar to those in Figure 15.

CONCLUSIONS

The effects of the water surface and the bottom of a basin on the vertical force and pitching moment experienced by an axisymmetric radio controlled model have been analyzed with a Reynolds-averaged Navier-Stokes code. Computations have been carried out for three submergence depths and 6 speeds.

The predicted force and moment vs. speed for three submergence depths are plotted in Figures 18 and 19. The values for $Fr = 0.077$ for all depths and for $Fr = 0.153$ for depths 10 and 13 are from double model solutions because this approximation is quite accurate for low speed and because of the difficulty encountered in obtaining free surface solutions at such low speeds. Also shown are values computed by using a potential flow code with free surface capability.*

*Y. Hong, private communication

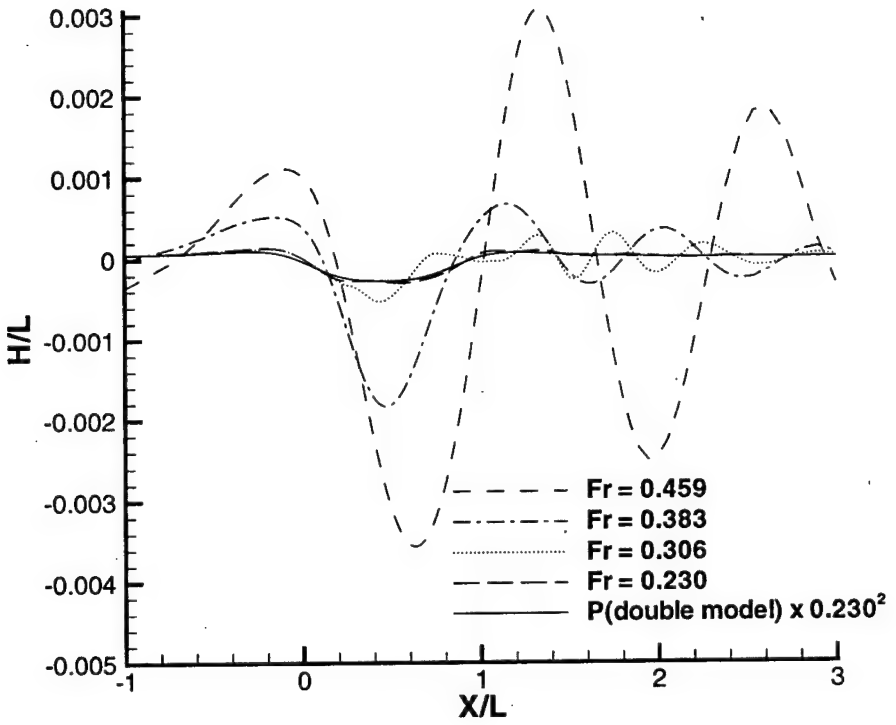

Fig. 15. Computed centerline wave profiles for depth 10 and four speeds compared with a profile obtained from a double model solution.

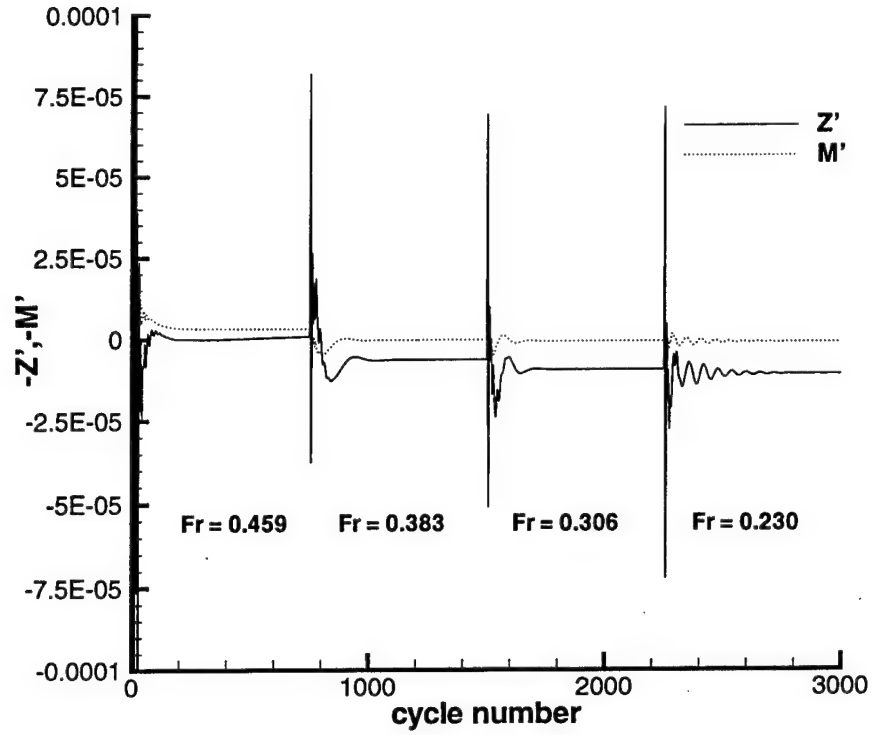

Fig. 16. Computed force and moment histories for depth 13 and four speeds.

Over the speed range considered, there is an attraction of the body toward both the water surface and the basin bottom. These attractive forces depend on the distances from the body to the bottom and to the water surface. For all but the highest speeds these forces are relatively small. At the lowest speeds the forces become essentially speed independent. In the low speed range the force due to the water surface is essentially the same as the force due to a wall. This is consistent with a double model solution being an accurate free-surface solution as the speed approaches zero. That this accuracy becomes excellent at the lower end of the speed range has been confirmed by carrying out double-model computations and comparing with the free-surface computations.

For higher speeds, the free-surface effect is evident in Figure 18. With increasing speed an enhanced attraction toward the water surface is noticeable for all depths and is particularly strong for depth 7. The reason for this increased vertical force is the shift of the surface waves downstream relative to the body as the speed increases. This shift results in a modification to the pressure field at the water surface which extends to the body.

The pitching moments are relatively small at the lower speeds (Figure 19). This is consistent with the fore and aft symmetry and the small amplitude of the wave pattern in the slow speed range. As the waves grow and shift downstream at higher speed an increasing bow-down moment is predicted at all depths. This coincides with a lowering

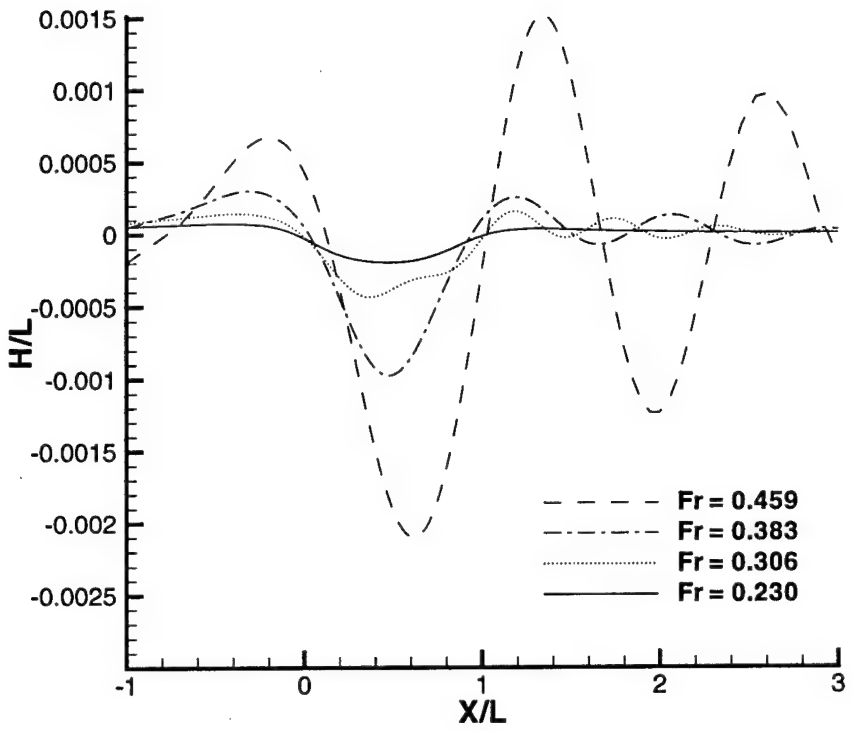

Fig. 17. Computed centerline wave profiles for depth 13 and four speeds.

of the pressure on much of the aft portion of the upper body surface due to the large surface trough.

The viscous and inviscid results show some differences. The predictions of the RANS code show somewhat more attraction toward the water surface and larger moments than those from the potential flow. The forces predicted by the potential flow at the two higher speeds for depth 7 deviate from the smoother pattern of the RANS results. Whether these differences are due to viscous effects is difficult to conclude. Perhaps some of the differences are due to inaccuracies in one or both of the solutions. Further studies would need to be done to assess this possibility. It might be supposed that viscous effects would be quite small. The free surface waves are an essentially inviscid phenomenon. The flow at the stern of the body does exhibit strong viscous effects including a thick boundary layer and a pressure distribution which is markedly different from that of potential flow. This difference in pressure distribution is vertically symmetric and therefore does not directly produce any vertical force. However, it could have some indirect influence on the force if it significantly effects the surface wave pattern.

The forces on the body computed here are not sufficient to account for the necessary sternplane deflections for straight and level motion near the water surface. However, it was shown that for depth 7 at the highest speed that local angles of attack on

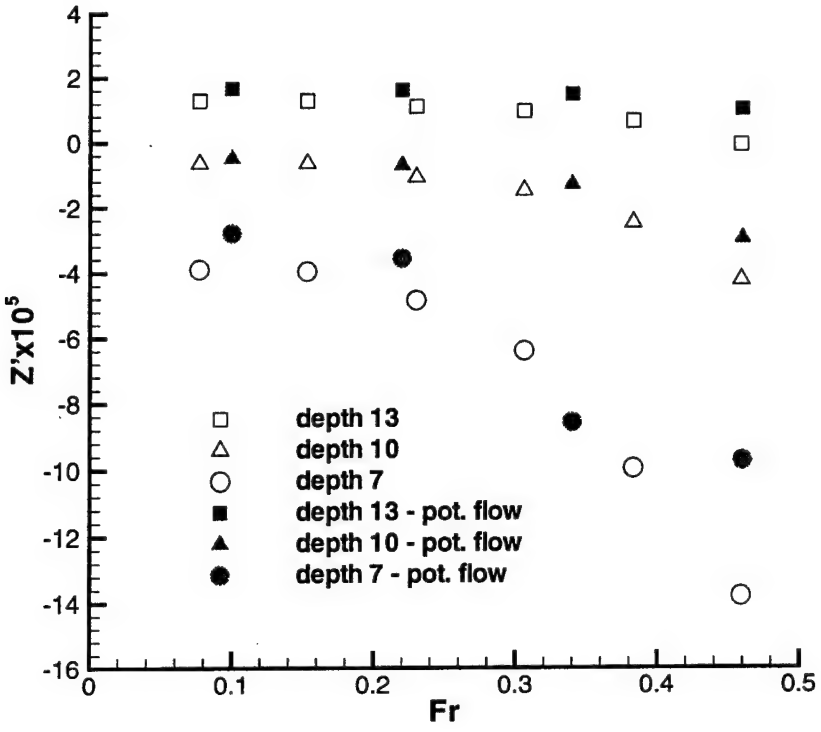

Fig. 18. Computed vertical force coefficient vs. Froude number for various submergence depths.

the order of 1 degree are achieved near the stern in the horizontal centerplane. This upwash is comparable to the 1 degree sternplane deflections needed to keep the RCM in straight and level motion at similar depths. The local angles of attack diminish with decreasing speed and with increasing depth of submergence as do the necessary sternplane deflections.

ACKNOWLEDGEMENTS

The authors hereby acknowledge the contributions of Mr. Thomas Moran and Dr. Ming Chang of NSWCCD, Code 5600 who requested the study and provided useful guidance throughout the effort. Computer time was provided by the DoD HPC Main Shared Resource Center at ARSC (Cray T3E).

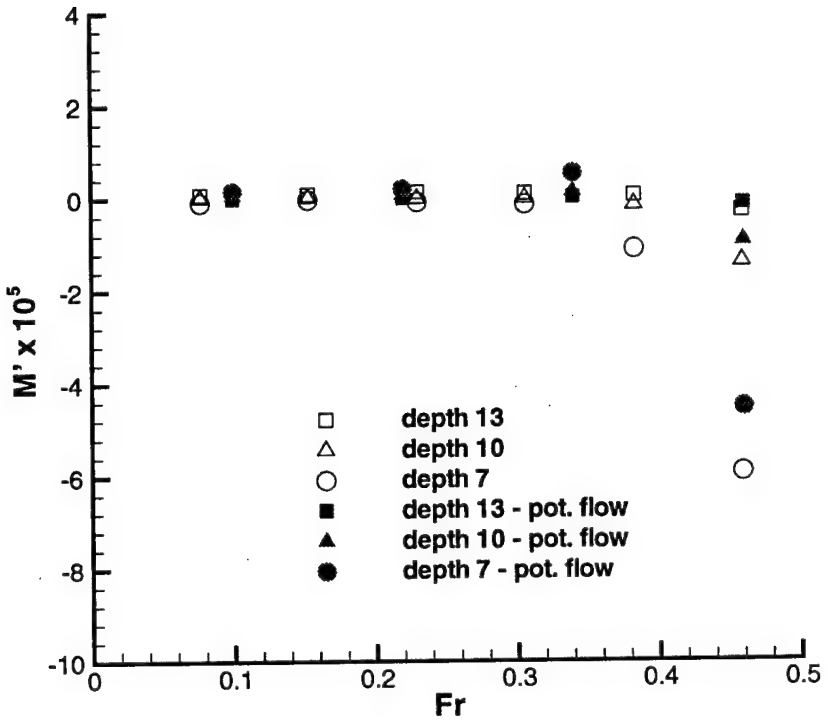

Fig. 19. Computed pitching moment coefficient vs. Froude number for various submergence depths.

THIS PAGE INTENTIONALLY LEFT BLANK

REFERENCES

1. Watkinson, K.W., Kueny, K.L., and Tureaud, T.F., "LSV Maneuvering Experiments: RCM Scaling Phenomena, LSV Test Results", Vehicle Control Technologies, Inc. Report No. 28, November 1996.

2. Tureaud, T.F., Yates, J.E., and Smith, N.S., "LSV Maneuvering Experiments: RCM Scaling Phenomena, Post Test Model Evaluation", Vehicle Control Technologies, Inc. Report No. 29, January 1997.

3. Massa, L. and Taylor, L.K., "Analysis of the Influence of the Bottom on the Hydrodynamic Forces Acting on DARPA SUBOFF Model," Mississippi State University, NSF Engineering Research Center for Computational Field Simulation, Report No. MSSU-COE-ERC-98-01, March 1998.

THIS PAGE INTENTIONALLY LEFT BLANK

INITIAL DISTRIBUTION

Copies		
4	ONR	
1	333	P. Purtell
1	333	E. Rood
1	334	G. Gebsen
1	334	A. Tucker
2	OPNAV	
1	N875	J. Schuster
1	N875F	E. Joyal
14	NAVSEA	
1	93R	D. Dahmer
1	93R	A. Spiro
1	PMS450	L. Becker
1	PMS450	J. Evans
1	PMS450	CAPT S. Petri
1	08	D. Blessing
1	08	J. Demko
1	08	J. Kearney
1	05HB	C. Crockett
1	05H	J. Fein
1	05H	M. King
1	05H	J. Leadmon
1	05HT	C. Merrill
1	05H	M. Nicholson
2	NUWC	
1		J. Meng
1		P. Lefebvre
2	DTIC	

Copies		
1	EB	
1		D. Panofsky
3	NNS	
1		J. Caspar
1		T. Huang
1		K. Smith
1	DARPA	
1		CAPT Polcari
5	Miss. State U.	
1		M. Beddhu
1		R. Briley
1		R. Pankajakshan
1		L. Taylor
1		D. Whitfield

CENTER DISTRIBUTION

Copies	Code	Name
1	0114	K.-H. Kim
1	27	D. Dozier
1	5010	B. Raver
6	5060	D. Walden
1	5080	R. Boswell
5	5400	R. Coleman
1	5400	J. Gorski
5	5400	H. Haussling
1	5400	F. Peterson

CENTER DISTRIBUTION (Cont.)

Copies	Code	Name
1	5600	M. Chang
1	5600	R. Curphey
1	5600	J. Feldman
1	5600	K. Junghans
1	5600	I.-Y. Koh
1	5600	T. Moran
1	3442	TIC